Fault-bend fold

A.

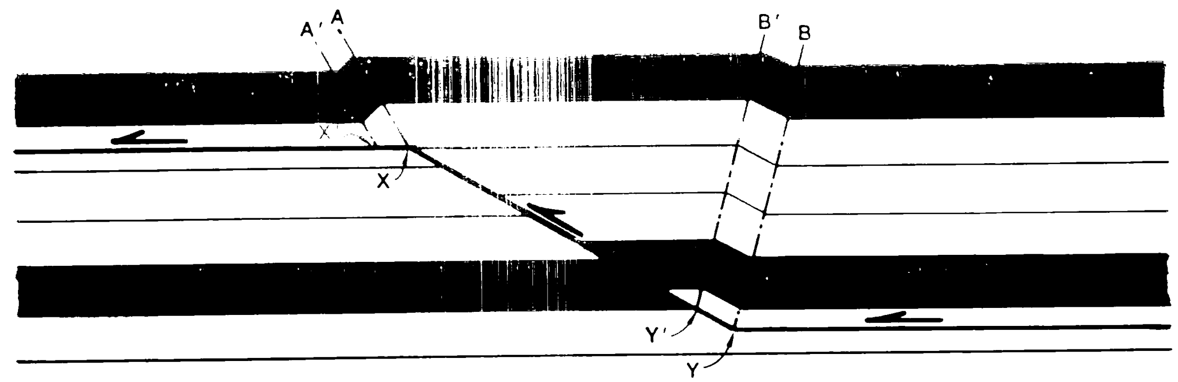

Suppe, 1983

Fault-bend fold

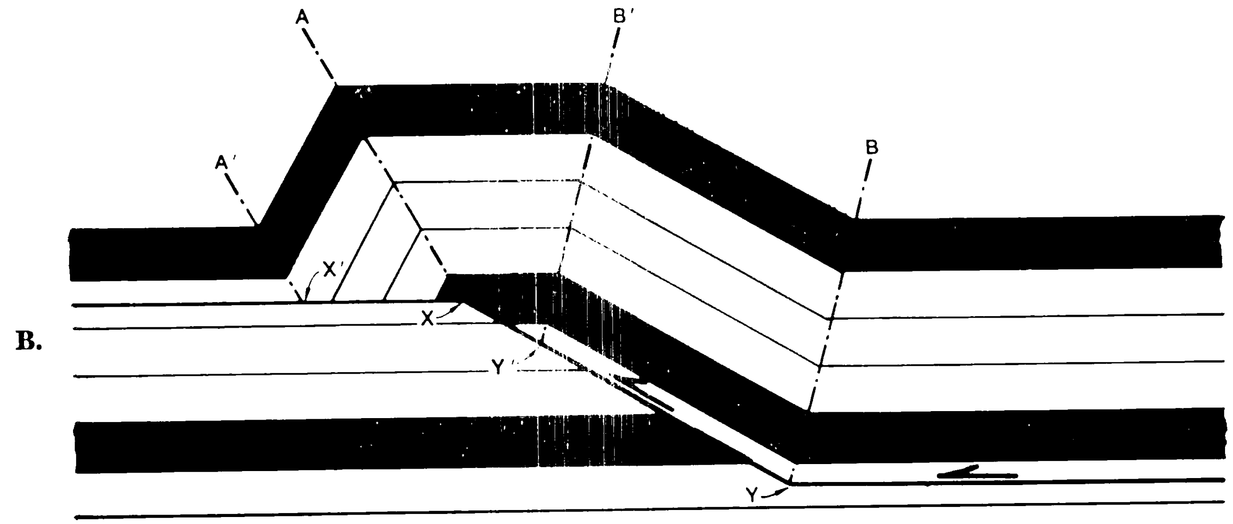

Suppe, 1983

Fault-bend fold

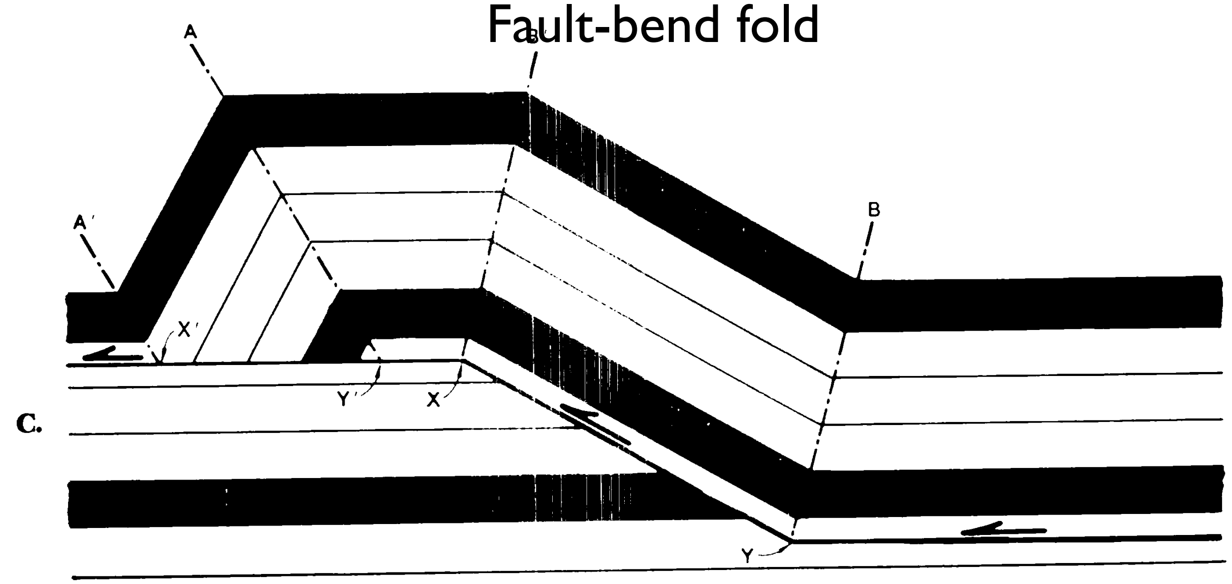

Advantages:

Can be reconstructed from surface geology

Assumptions:

Pervasive slip on bedding planes as rocks pass through hinges

Slip is carried off-section (no deformation of lower plate)

Suppe, 1983

Fault-Propagation fold

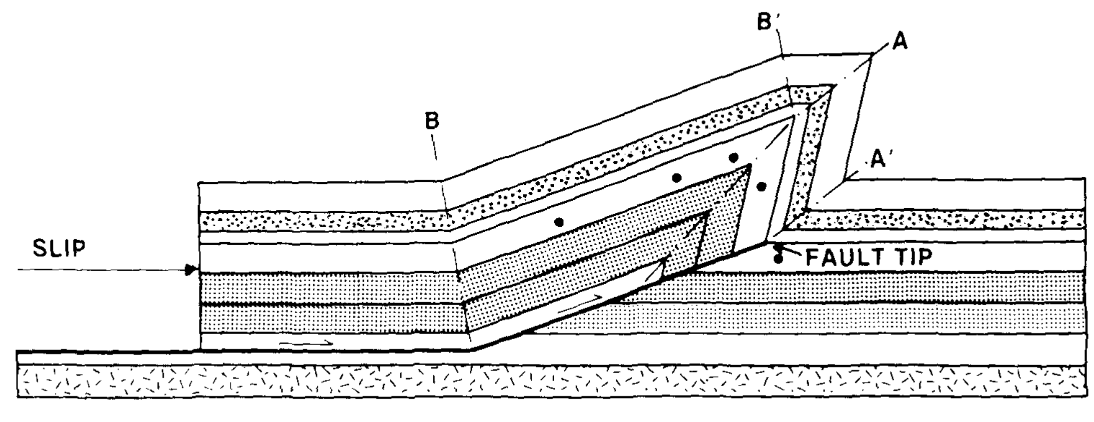

Namson and Davis, GSA Bull , 1988 after Suppe and Medwedeff, 1984

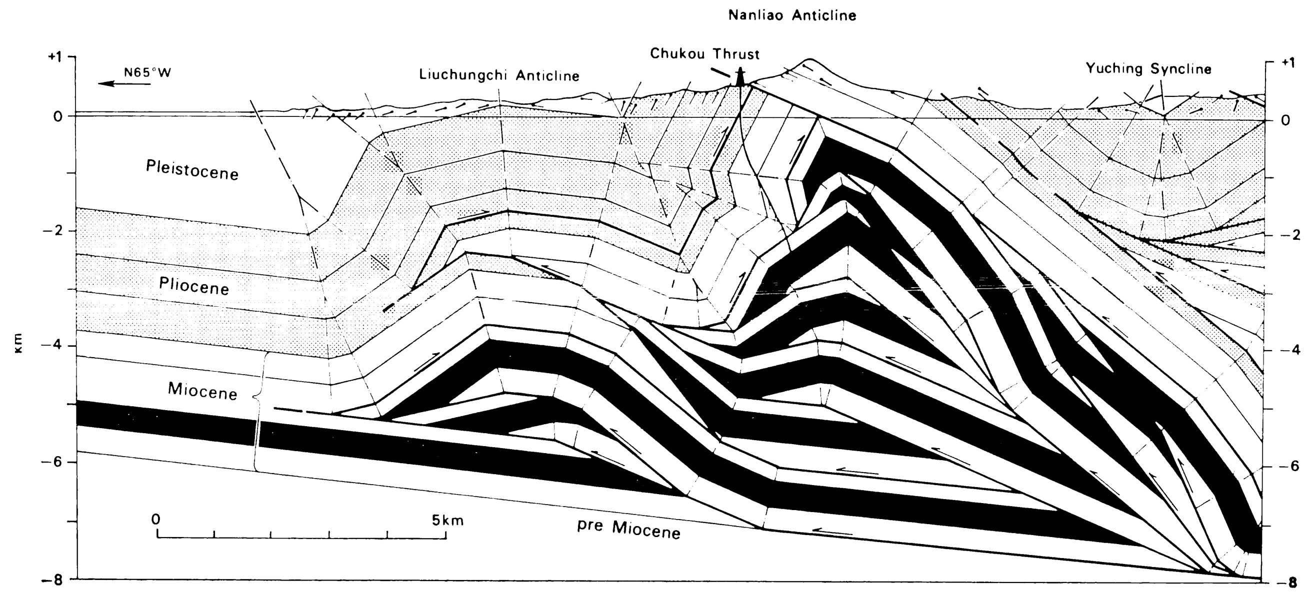

Fig. 24. Structural interpretation of the Nanliao anticline, southern Taiwan (modified from Suppe, 1980b).

Suppe, 1983

Coalinga, California (site of 1983 earthquake)

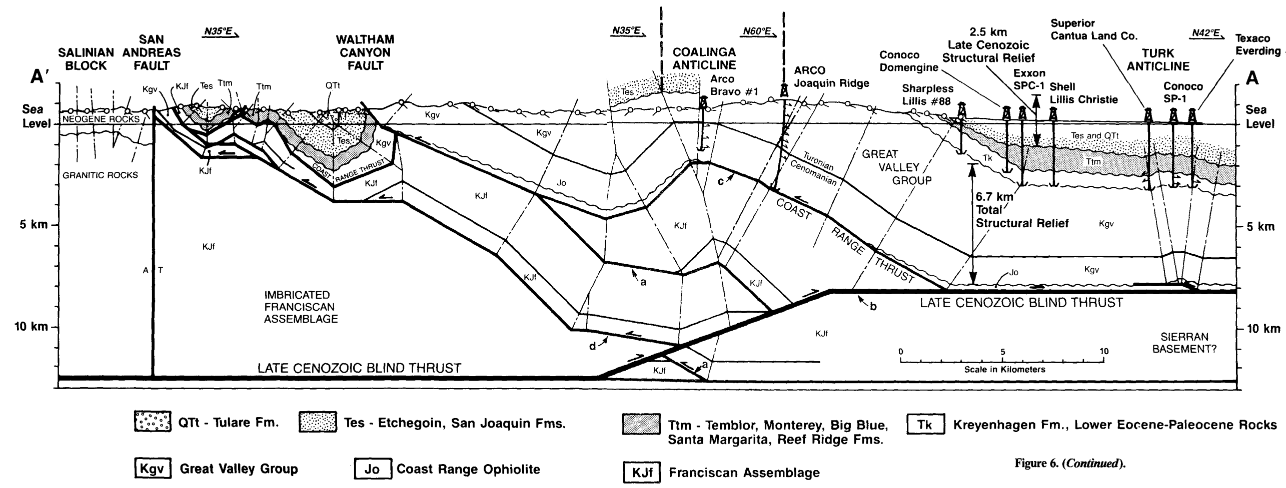

Figure 6. (*Continued*).

Namson and Davis, GSA Bull , 1988

Coalinga anticline grew in the earthquake, which lacked any surface faulting.

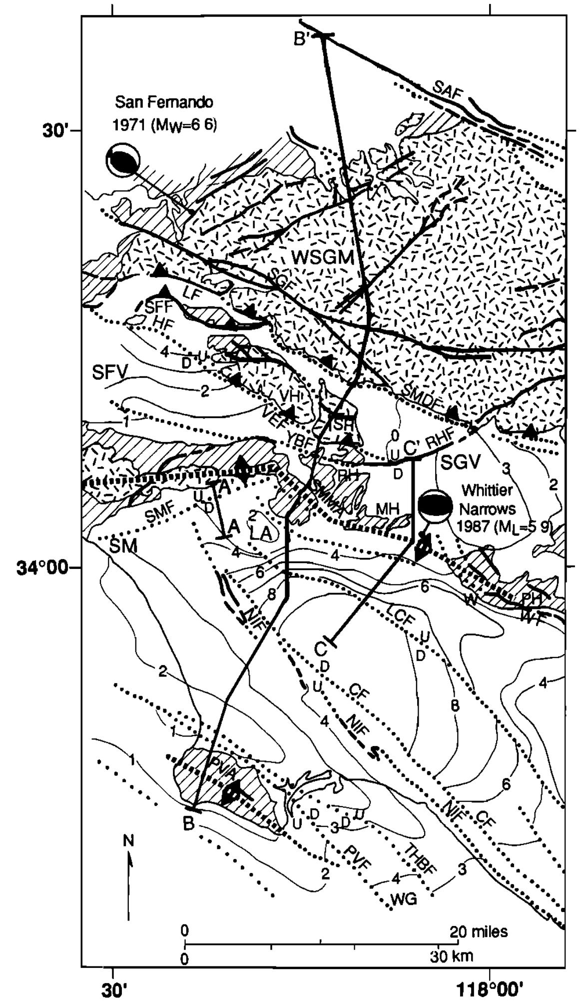

Davis et al., JGR, 1989

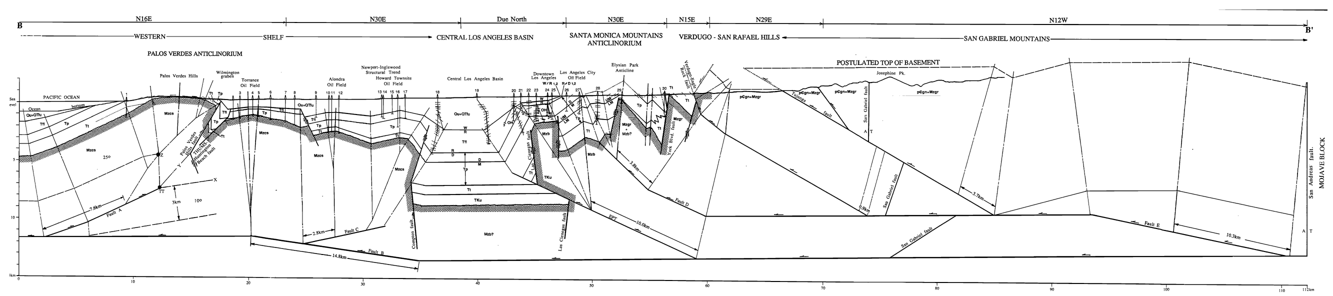

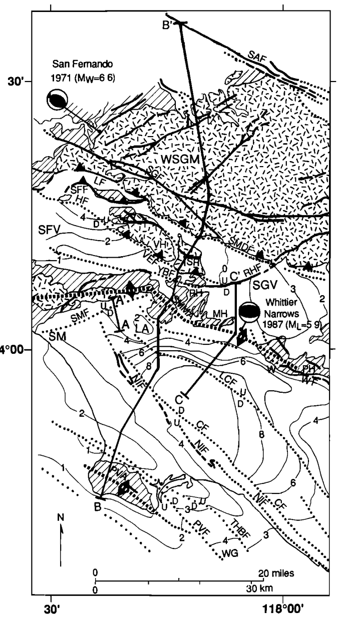

Davis et al., JGR, 1989

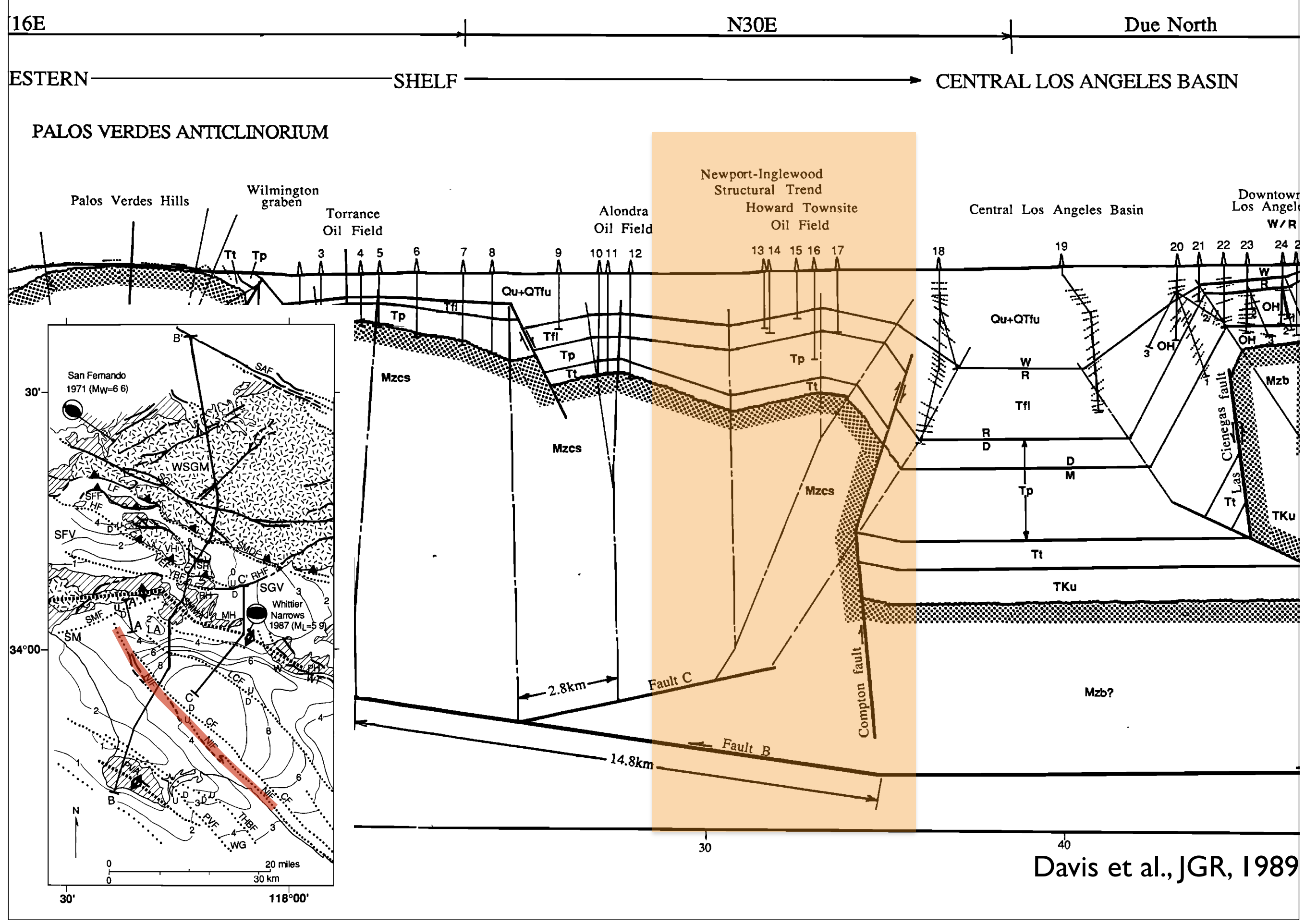

Davis et al., JGR, 1989

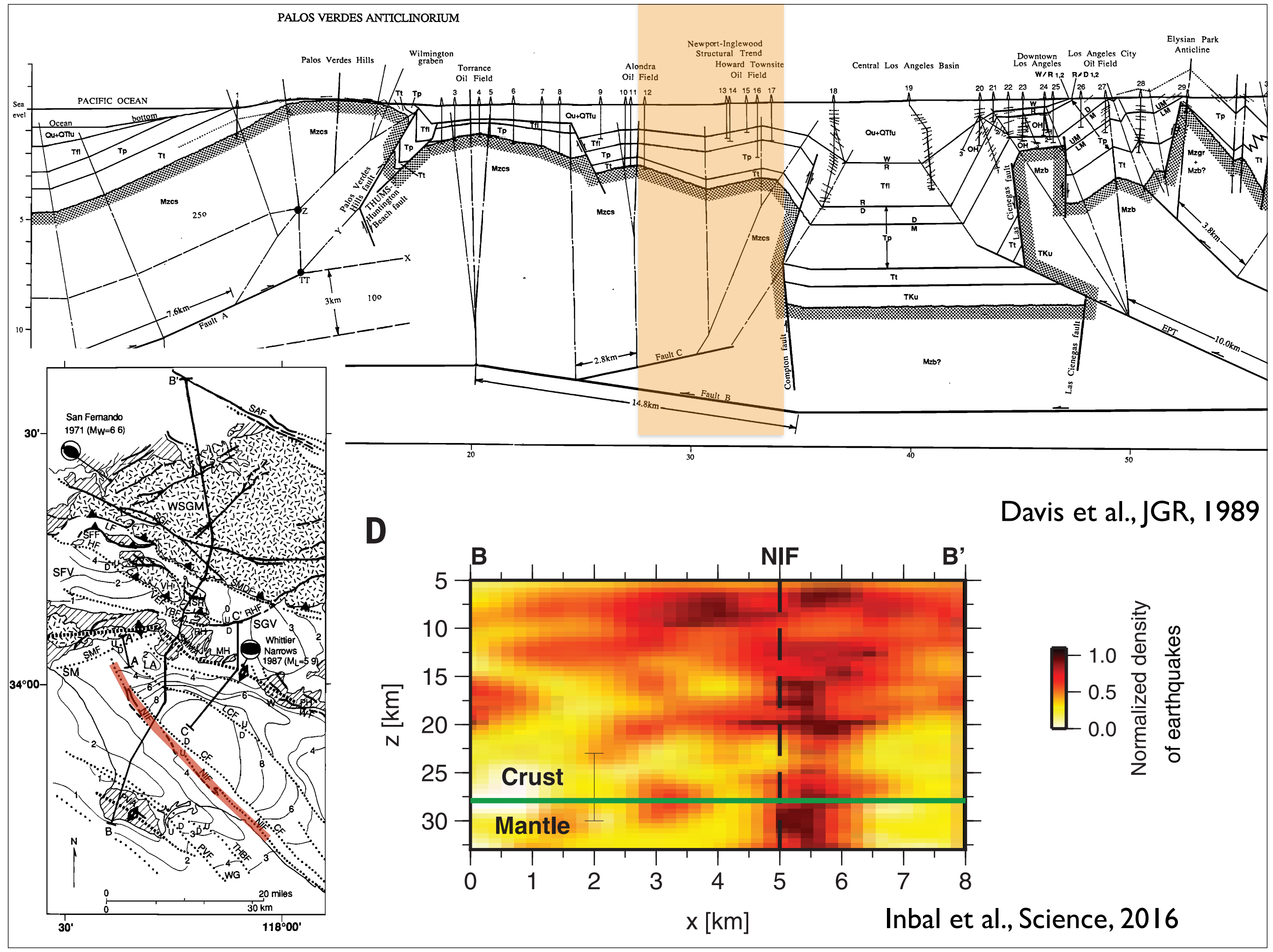

Inbal et al. got lots of small EQs from a very dense array and see the Newport-Inglewood fault extending into the mantle, not detached as thought by Davis et al. This helps reveal a weakness of the geometric reconstructions of fold belts: they need detachment to go off the edge of the model at the side.

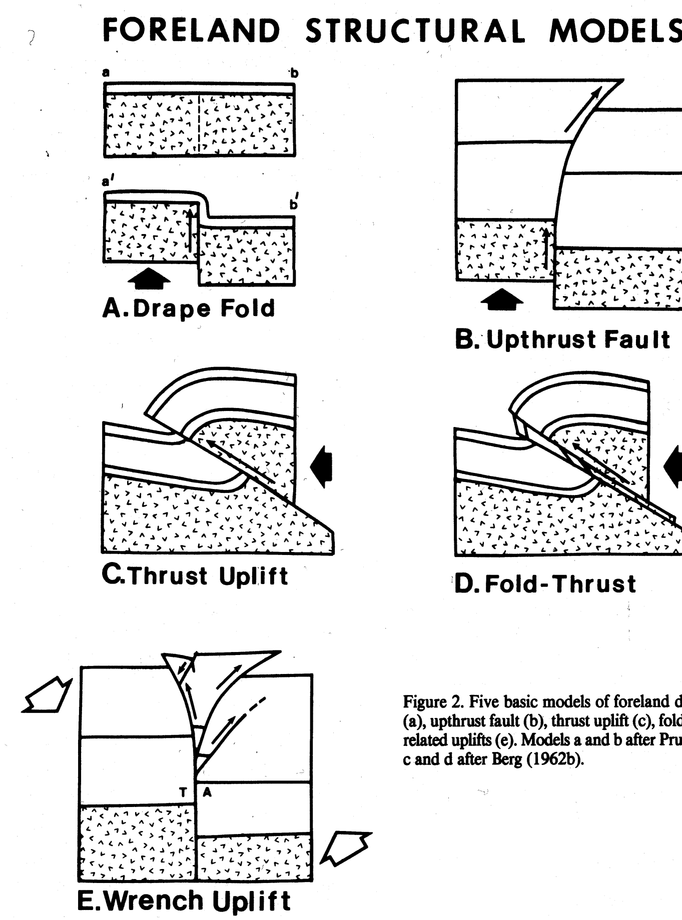

Figure 2. Five basic models of foreland deformation are the drape fold (a), upthrust fault (b), thrust uplift (c), fold-thrust uplift (d), and wrench-related uplifts (e). Models a and b after Prucha and others (1965); models c and d after Berg (1962b).

Brown, GSA Mem 171, 1988

Well, as a prelude to the Laramide, let's discuss a different flavor of this: basement cored folds.

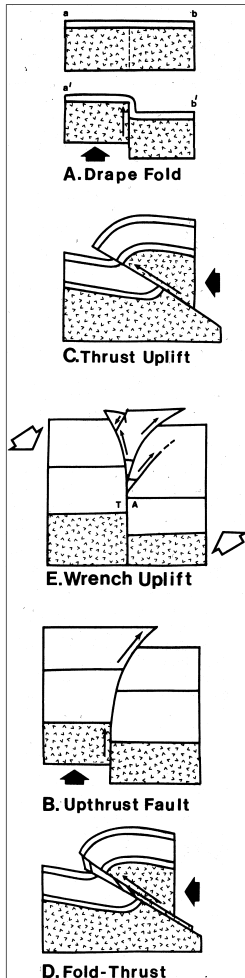

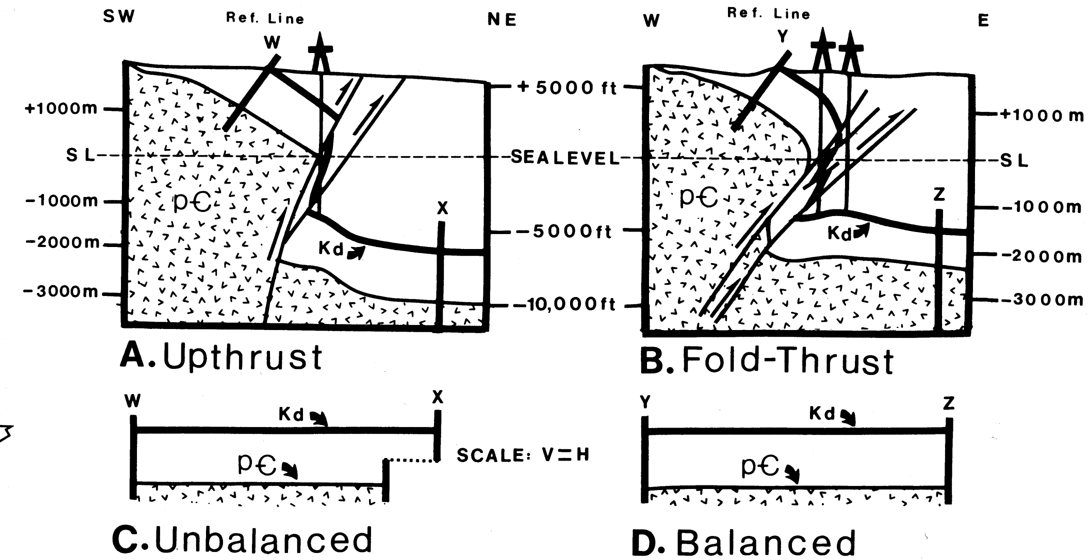

Figure 5. A comparison of interpretations of the Soda Lakes area, Colorado, utilizing the upthrust model (a) modified from Osterwald (1961), and the fold-thrust model (b) modified from Berg (1962a). Comparison of bed-length measurements of the Dakota Sandstone (Kd) and the top of the Precambrian basement between reference lines (W-X), and (Y-Z), indicates the upthrust model (c) is out of structural balance by approximately 20 percent, whereas the fold-thrust model (d) is balanced to less than 5 percent error (after Brown, 1987).

Brown, GSA Mem 171, 1988

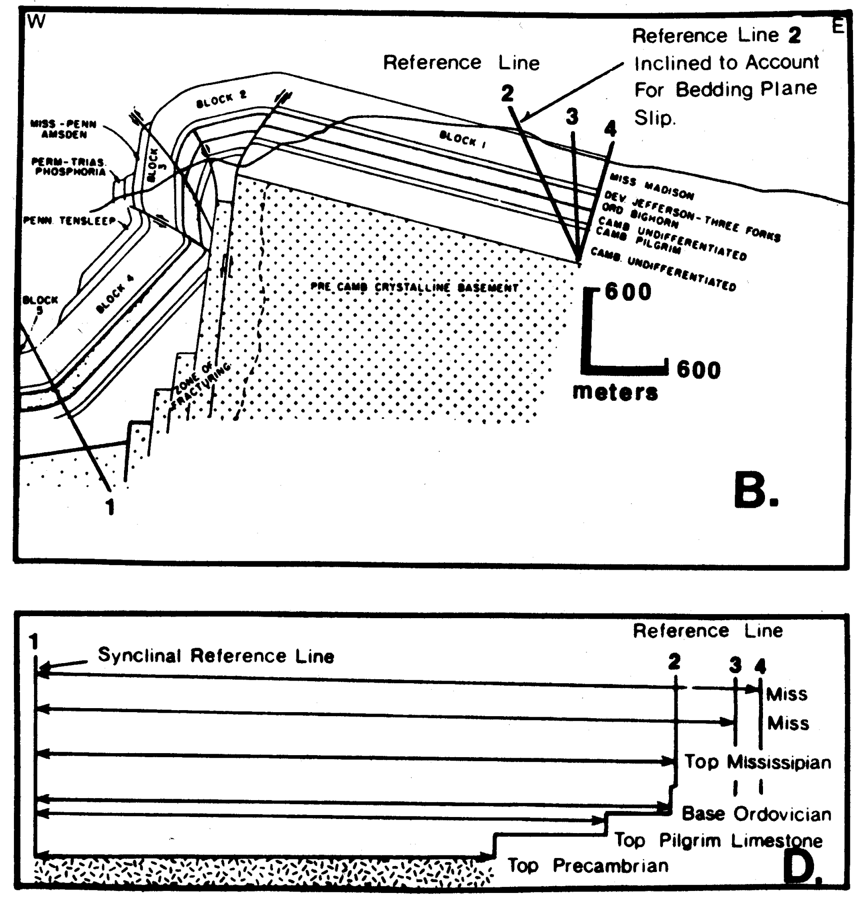

Rattlesnake Mtn interpretation of Sterns, 1971

Brown, GSA Mem 171, 1988

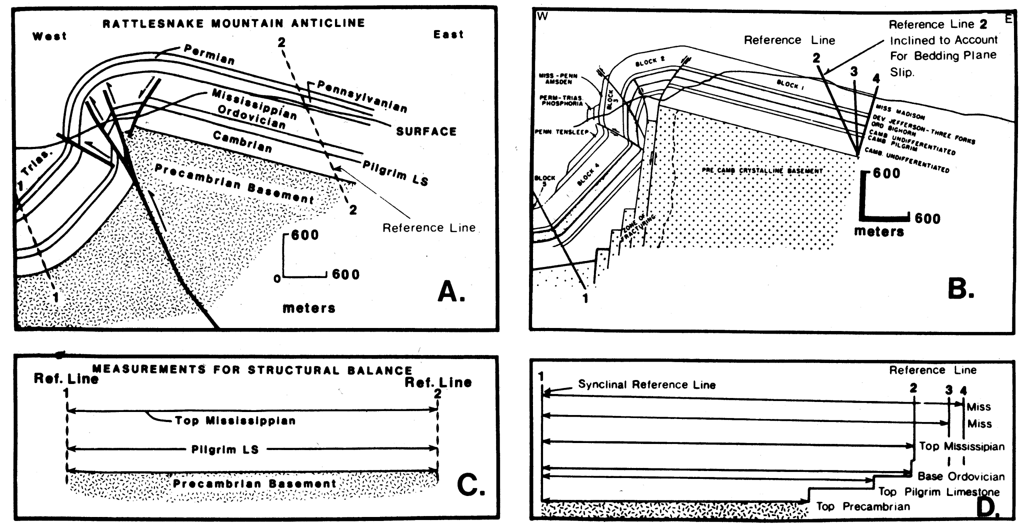

Rattlesnake Mtn interpretation of Brown, 1984

Rattlesnake Mtn interpretation of Sterns, 1971

Brown, GSA Mem 171, 1988

Brown, GSA Mem 171, 1988

Rattlesnake Mtn interpretation of Brown, 1984

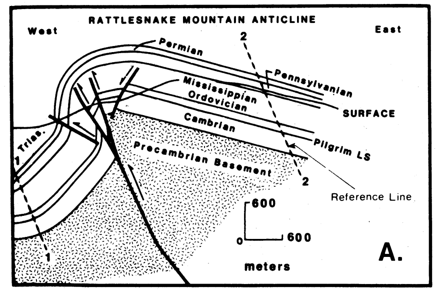

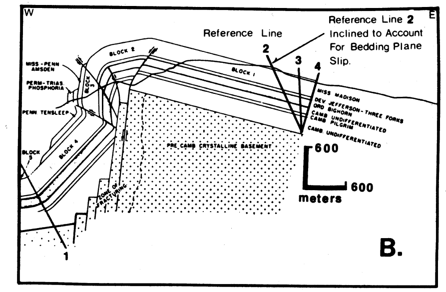

Rattlesnake Mtn interpretation of Sterns, 1971

Rattlesnake Mtn interpretation of Erslev, 1986

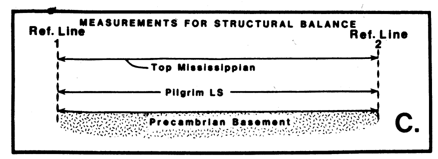

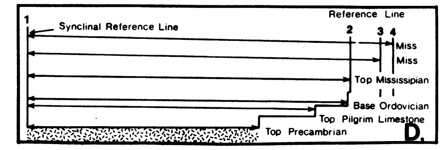

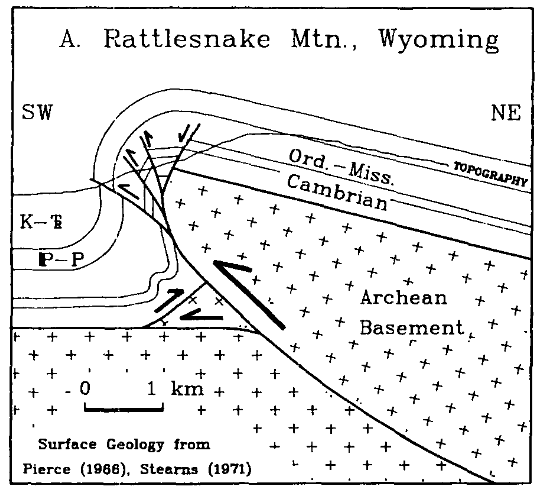

B. Fault Dip Calculation

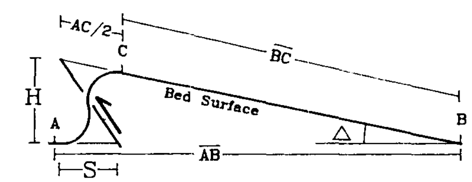

$\triangle$ = Hanging Wall Dip − Footwall Dip

AC and AB Are Bed Lengths

$H = (\overline{BC} + AC/2)\sin\triangle$

S = Total Shortening − Tilt Shortening

$S = AB - \overline{AB} - (\overline{BC} + AC/2)(1 - \cos\triangle)$

Fault Dip Relative to Footwall = arctan (H/S)

Erslev, Geology, 1986

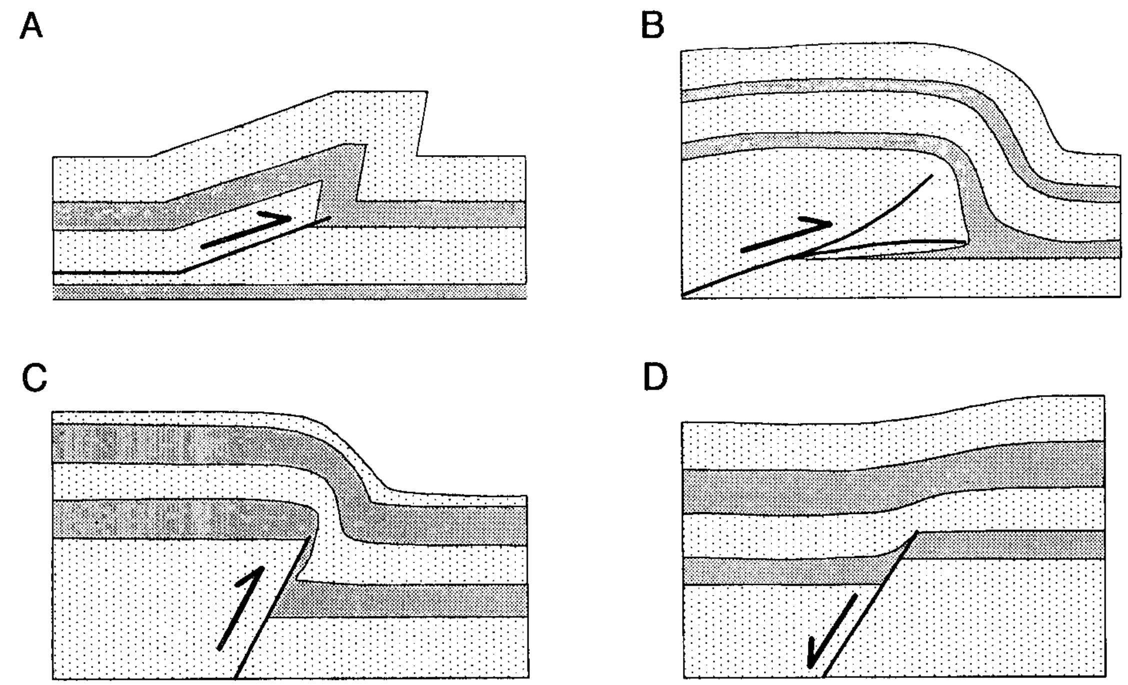

Figure 1. Models of fault-propagation folds. A: Geometric kink-band model (Suppe and Medwedeff, 1984). B, C, D: Analog experimental models of folds above thrust (B; Chester et al., 1988), reverse (C; Friedman et al., 1980), and normal (D; Withjack et al., 1990) faults.

Erslev, 1991

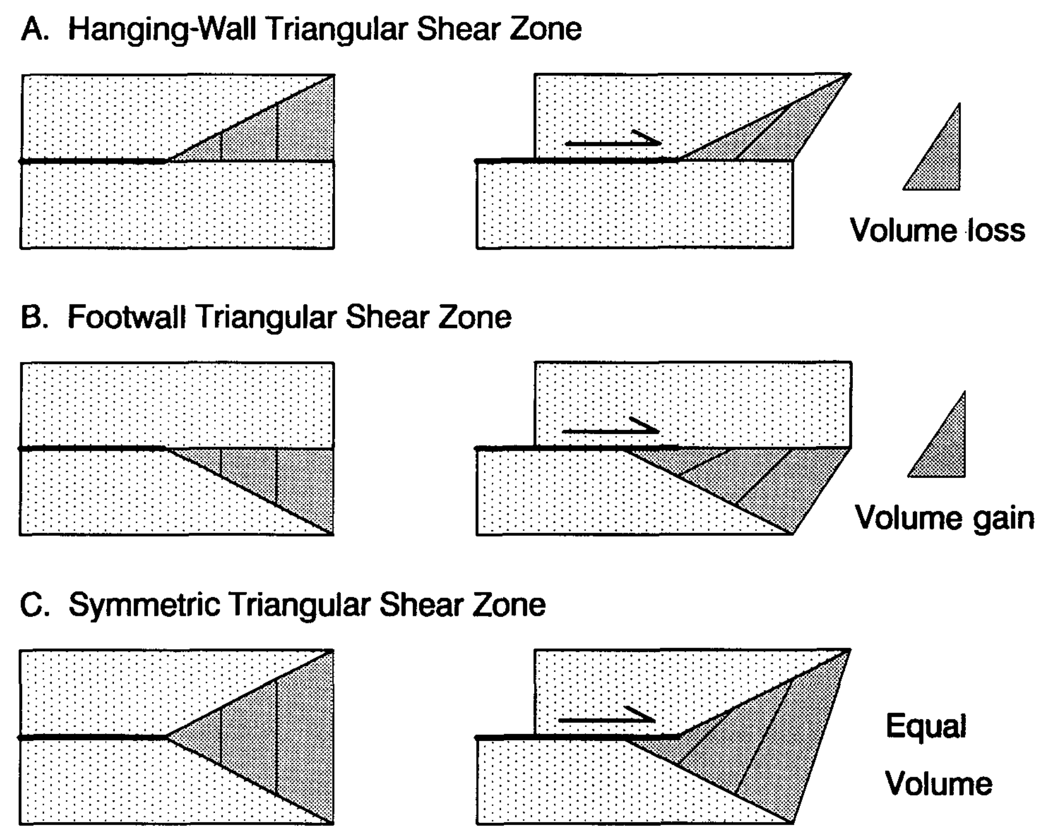

Figure 2. Geometric end members of triangular shear-zone folding.

Erslev, 1991

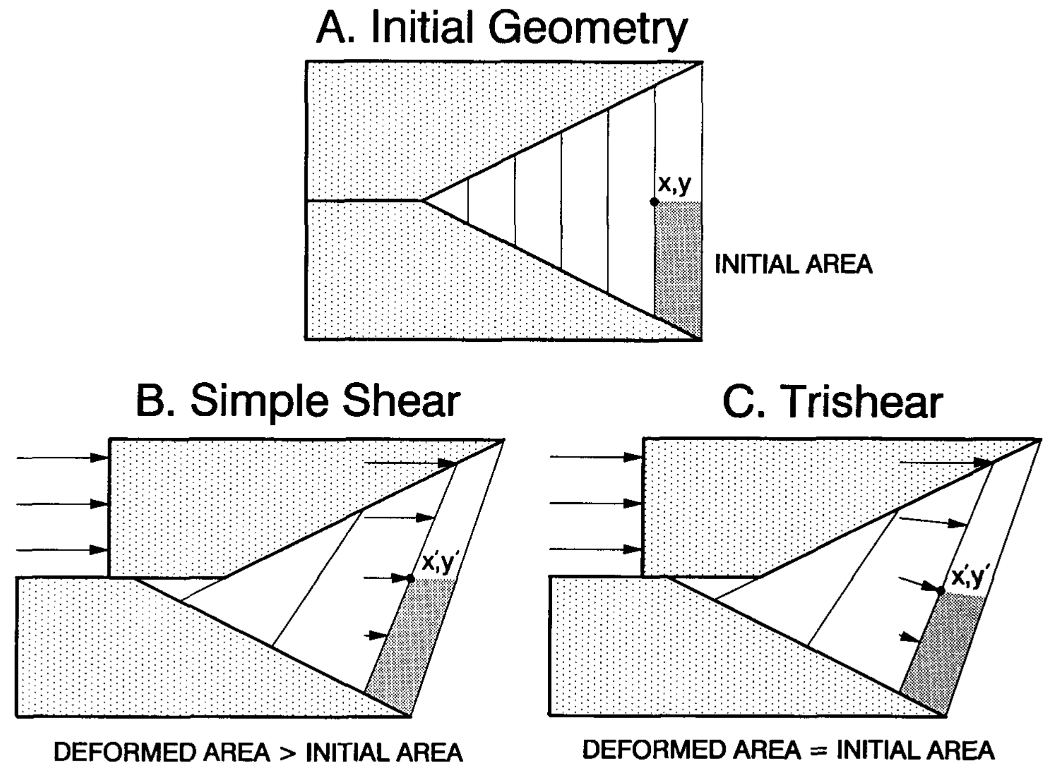

Figure 3. Simple shear and trishear approximations of homogeneous shear in triangular shear zones.

Erslev, 1991

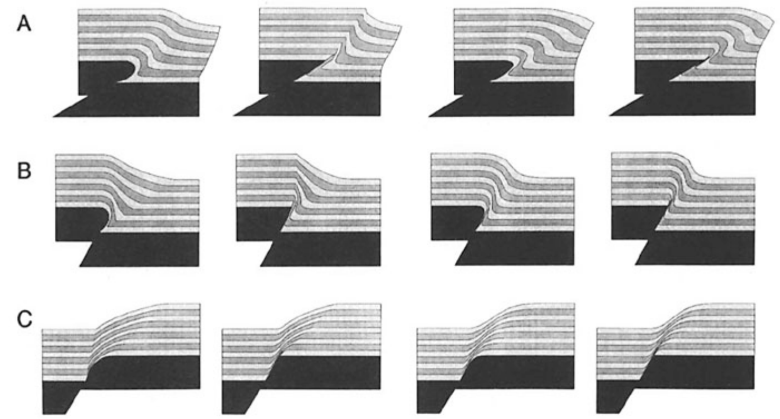

Figure 4. TRISHEAR-generated, homogeneous and heterogeneous fault-propagation folding above (A) thrust (30° dip, 60° apex angle), (B) reverse (60° dip, 60° apex angle), and (C) normal (60° dip, 40° apex angle) faults.

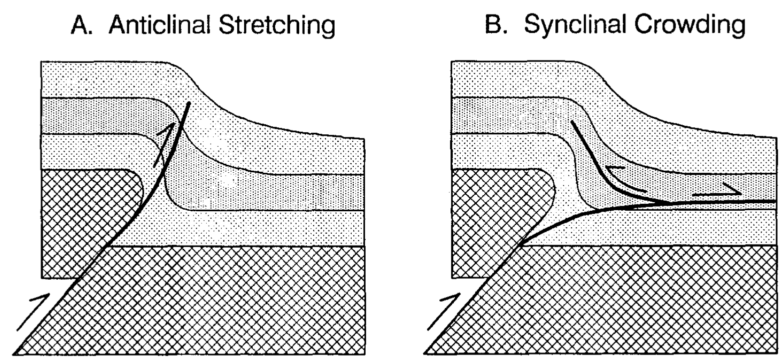

Figure 5. Fault-propagation trajectories suggested by homogeneous, footwall-fixed trishear in front of thrust faults (45° dip, 60°apex angle).

Advantages:
- Deals with more realistic geometries in foreland situations than fault-bend folds

Disadvantages:
- Requires plastic deformation in trishear zone, which can become non-unique in terms of structures

Erslev, 1991

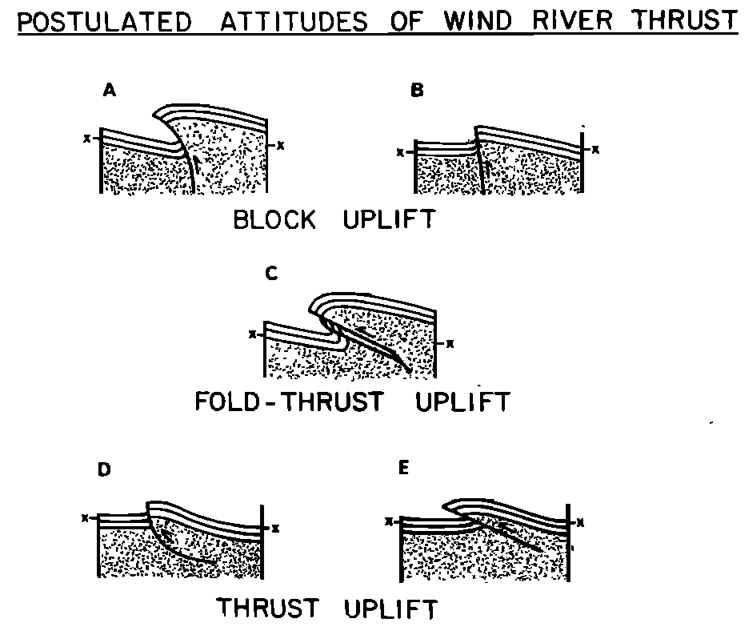

Fig. 1. Proposed structural styles for the Wind River fault. Structure between that in Figure 1c and in 1e is representative of the fault at depth; x-x represents the position of the present ground surface.

Smithson et al., JGR, 1979

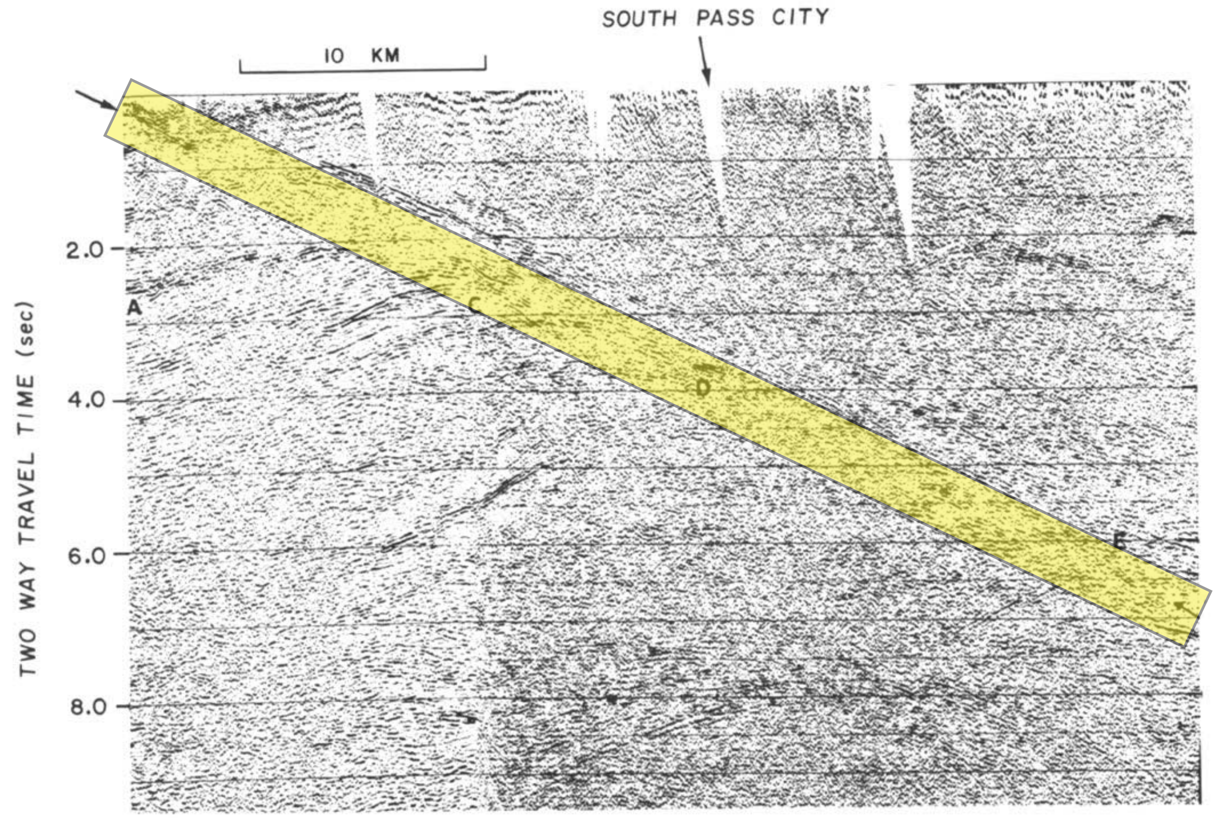

Figure 3. Unmigrated 24-fold CDP stacked reflection profile representing the upper portion of the Wind River thrust. Arrows define the position of the events representing reflections from the thrust plane. A = reflections from flat-lying sediments of Green River Basin. C = uplift (in line sections) of sedimentary reflectors under fault with no evidence of overturning. D = position of thrust against base of sediments. E = thrust reflection in the Precambrian crystalline rocks of the crust.

Smithson et al., Geology, 1978

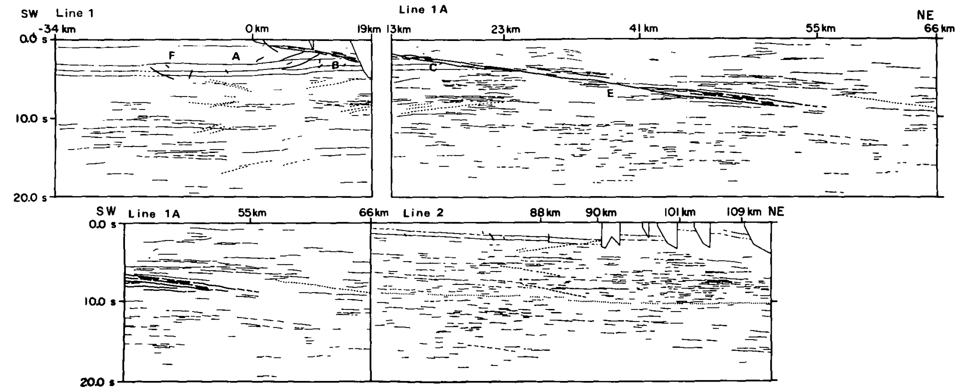

Figure 4. Interpretation of events seen on all three COCORP profiles. There is an overlap from the top northeast to bottom southwest parts of the diagram. The position of the Wind River thrust at the surface is represented by 0 km. The profiles were recorded to 20-s two-way traveltime. Dashed events represent diffractions or off-line reflections. A = reflections from flat-lying sediments of the Green River Basin. B = uplift (in time sections) of sediments underlying the Precambrian thrust over them by the Wind River thrust. C = termination of sedimentary layers against thrust with no evidence of overturning. E = appearance of thrust in the Precambrian crystalline rocks of the crust. Dotted lines represent enigmatic low-frequency event.

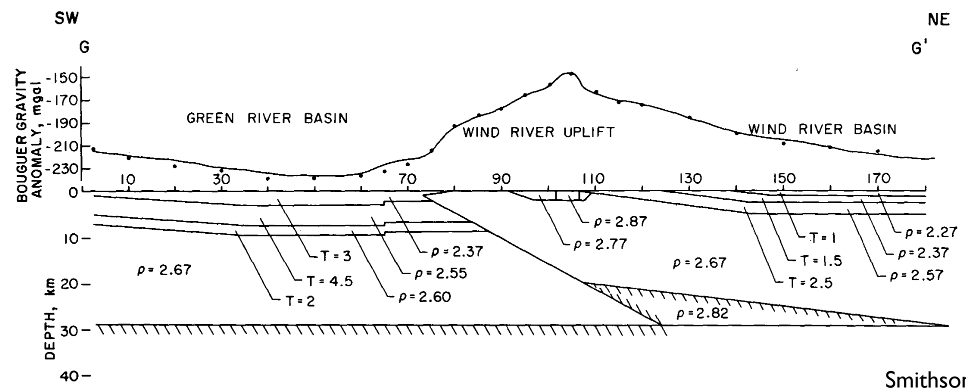

Smithson et al., Geology, 1978

Figure 5. Bouguer gravity anomalies and calculated model. Horizontal and vertical scale in kilometres. T = thickness of layers in kilometres; ρ = density in g/cm^3. Continuous line represents observed gravity. Dots represent modeled gravity.

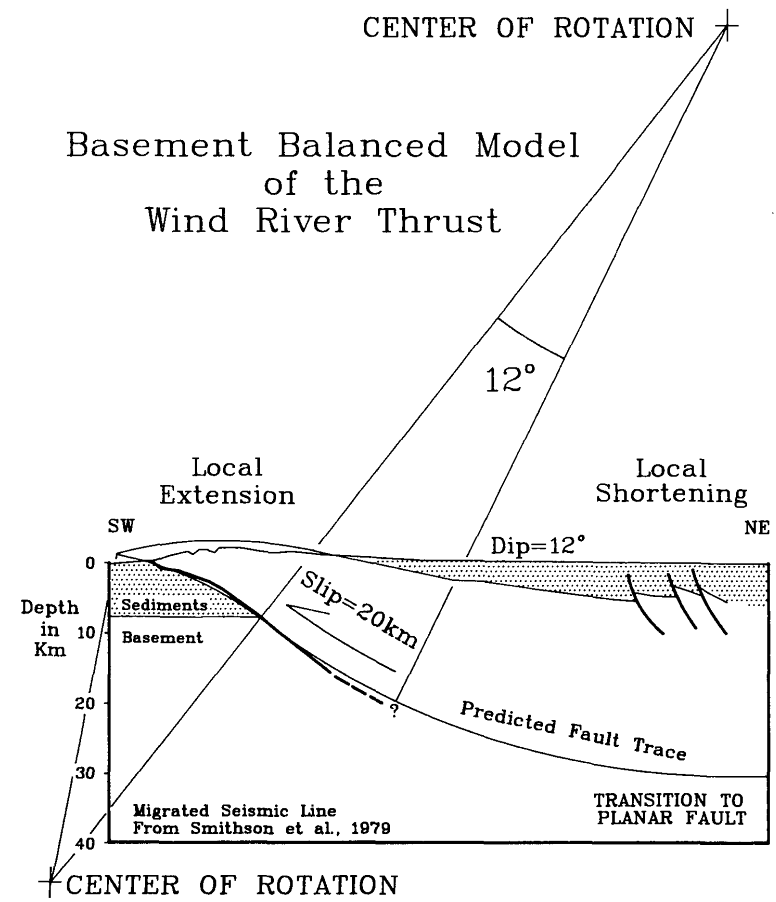

Figure 4. Illustration of congruency between seismic reflection data on Wind River thrust, Wyoming, and structural modeling discussed in text.

Erslev, Geology, 1986

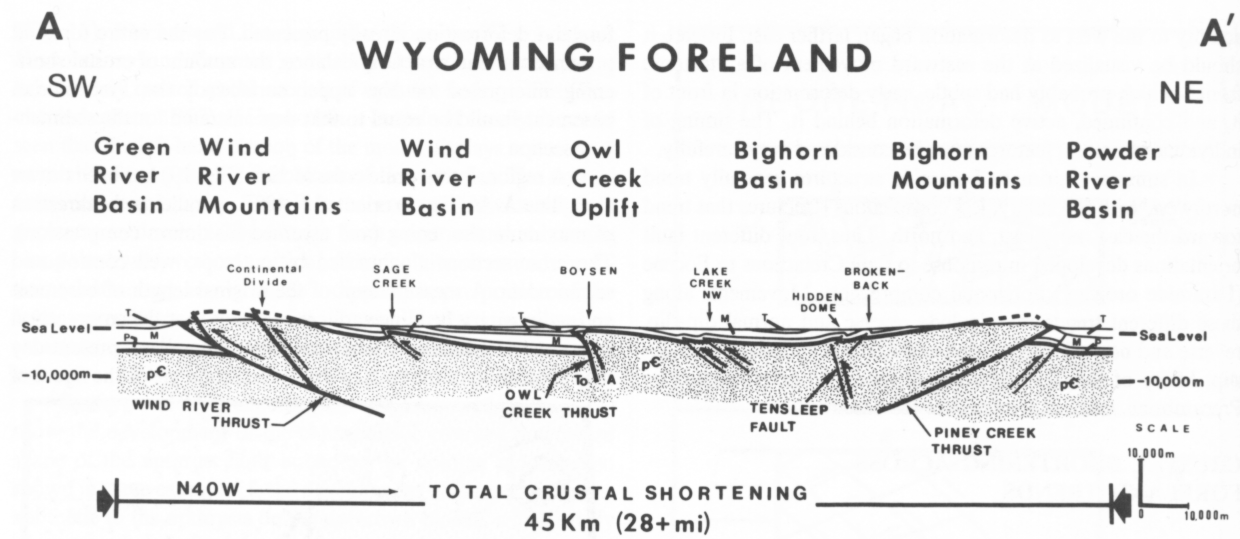

Figure 19. Regional true-scale structural cross section (line A-A′, Fig. 1) drawn parallel to direction of shortening and assumed direction of maximum compression (N.40°E.), demonstrates the conjugate nature of major foreland crustal faults. Different strike orientations of foreland structures result in differing amounts of crustal shortening, as shown by crossing the east-west–trending Owl Creek thrust and Tensleep fault, as compared to the northwest-trending Wind River thrust and the Piney Creek thrust in the Bighorn Mountains. Total crustal shortening along this line of section is 45 km (about 28 mi). T = Tertiary; M = Mesozoic; P = Paleozoic; p€ = Precambrian basement complex; To = toward; A = away.

Brown, GSA Mem 171, 1988

Other shortening estimates: 60-120 km by Chapin and Cather (1983) to NNE

43-52 km to ENE (Bird, 1998)

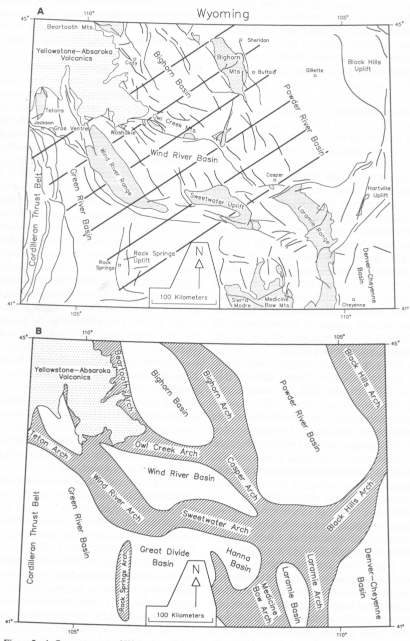

Figure 2. A: Structure map of Wyoming (after Blackstone, 1990a) with faults in finer lines and folds in thicker lines. Thick, broken straight lines show the cross-section lines for Figure 12. B: Arches and basins in Wyoming illustrating the connections between Rocky Mountain foreland culminations.

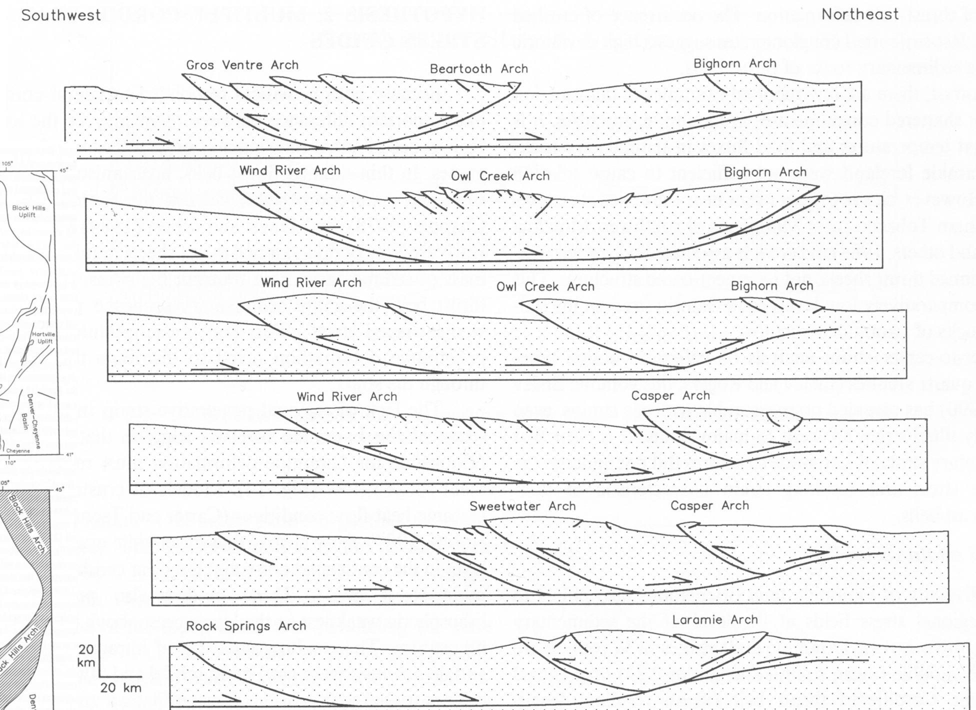

Figure 12. True-scale cross sections of the Precambrian basement surface in Wyoming (after Blackstone, 1990a) on lines shown in Figure 2A. These sections assume delamination in the lower crust and a uniform crust-mantle interface at 40 km below sea level. All fault geometries in the lower crust are schematic yet restorable in concept.

Erslev, GSA SP 280, 1993

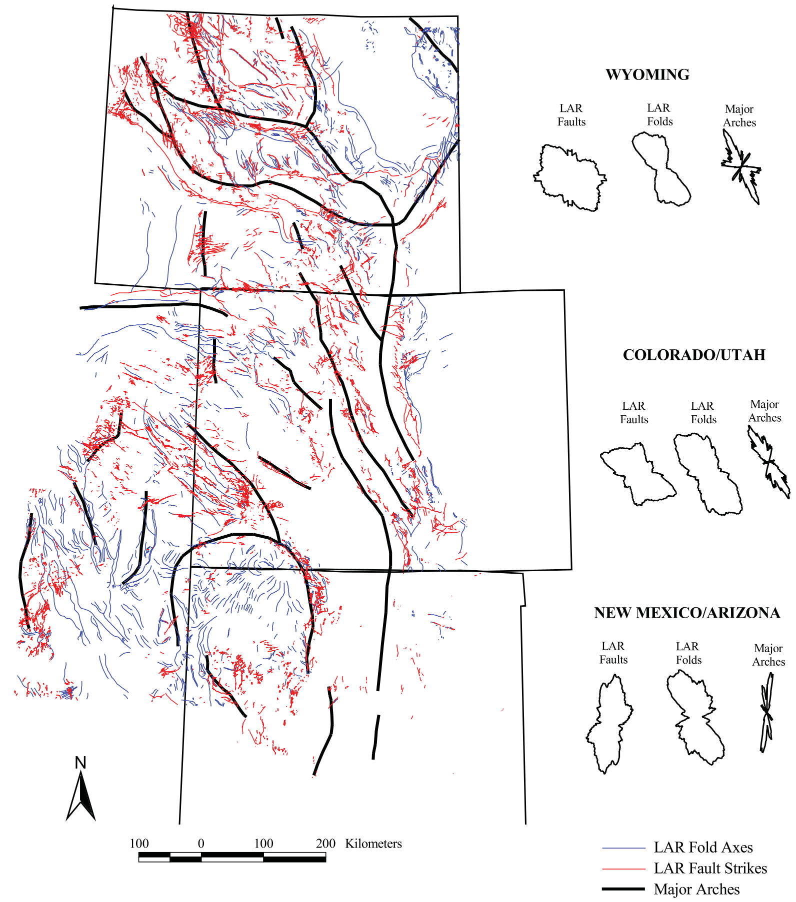

Figure 5. Map and rose diagrams of LAR arches, faults, and folds in Wyoming, Colorado-Utah, and New Mexico–Arizona.

Erslev, & Koenig, GSA Mem 204, 2009

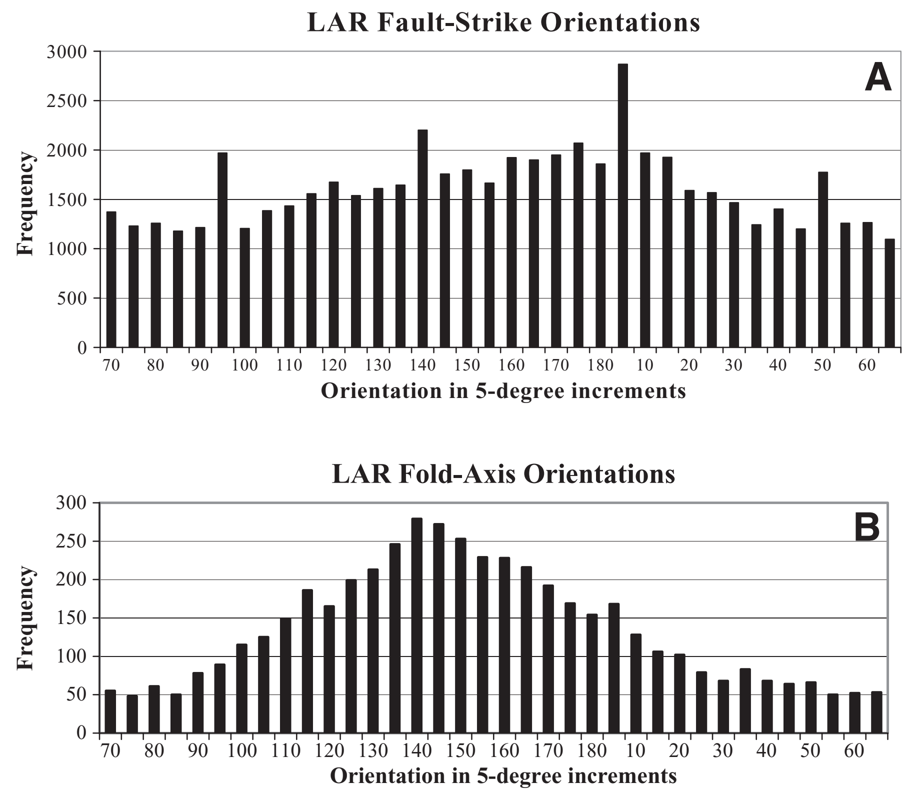

Figure 9. Histograms for all digitized LAR faults and folds from 0° to 180° in 5° increments.

Erslev, & Koenig, GSA Mem 204, 2009